Defect and Diffusion Forum
ISSN: 1662-9507, Vol. 451, pp 1-10
doi:10.4028/p-5rElXG

Submitted: 2025-12-12
Revised: 2026-02-20
Accepted: 2026-02-25
Online: 2026-04-17

Numerical Multiphysics CFD Modelling of Porosity Evolution in Thermoset Prepreg Microstructures

Anne-Lise Briard[1,2,a*], Raffaele D'Elia[1], Florentin Berthet[1], Anthony Cheruet[2] and Fabrice Schmidt[1]

[1]Institut Clément Ader (ICA)
Univ Toulouse, IMT Mines Albi, INSA Toulouse, ISAE Sup Aero, CNRS, ICA, Albi France

[2]Airbus Operations SAS
316 route de Bayonne, 31300 Toulouse, France

[a]anne-lise.briard@mines-albi.fr (*corresponding author), [b]raffaele.delia@mines-albi.fr, [c]florentin.berthet@mines-albi.fr, [d]anthony.cheruet@airbus.com, [e]fabrice.schmidt@mines-albi.fr

Keywords: Porosity, Thermoset Prepreg, Flow Simulation, Porous Medium.

Abstract. Carbon Fiber Reinforced Polymers (CFRPs) are essential to the aerospace industry, offering superior strength-to-weight ratios. Currently, the manufacturing of primary structures via standard autoclave curing is a robust, mastered process that successfully minimizes defects, keeping porosity levels below critical thresholds (typically < 1 %). Consequently, porosity is generally not considered as an issue in standard, optimized production lines.

However, this stability may be affected by emerging industrial paradigms aimed at increasing production rates and reducing costs. The shift toward accelerated manufacturing – characterized by rapid heating rates, shortened cure cycles and by new manufacturing processes – and the introduction of complex material architectures risk re-introducing significant porosity. In parallel, there is currently no numerical model capable of accurately predicting porosity formation and evolution under these complex conditions. Existing simulation approaches are typically macroscopic and rely on homogenized porous media assumptions, failing to capture the essential micro-scale interactions between bubbles and fibres.

To address this gap, this study presents an extended, custom multi-physics Computational Fluid Dynamics (CFD) solver built upon an existing OpenFOAM framework. The goal is to provide the first predictive tool for void evolution within realistic microstructures. The numerical framework couples a two-phase compressible flow model with the complete thermo-chemo-rheological physics of thermoset curing.

The solver is applied to 2D Representative Volume Elements (RVEs) of a prepreg ply. Simulations of a standard autoclave cycle demonstrated the solver's ability to capture micro-scale dynamics, showing how voids are compressed and transported during the resin viscosity drop before being frozen at gelation. A parametric study comparing 3-bars and 7-bars pressures confirmed the model's physical ability in predicting void volume reduction.

While currently focused on mechanical compression, the tool is designed to support the development of future manufacturing cycles. Future work will incorporate moisture diffusion physics and includes experimental validation via X-ray micro-tomography and in-situ synchrotron monitoring.

Introduction

Carbon Fiber Reinforced Polymers (CFRPs) are indispensable materials in the aerospace industry, offering exceptional strength-to-weight and stiffness-to-weight ratios. For primary structural components, thermosetting prepregs (e.g., carbon fibre reinforced epoxy) processed via autoclave curing remain the benchmark for achieving high performance, excellent consolidation, and minimal defect content [1].

Among all manufacturing defects, porosity (i.e. the presence of voids) is considered one of the most detrimental [1]. Voids, even at low volume fractions (1-2 %), act as stress concentrators,

promoting damage initiation and propagation. They significantly degrade matrix-dominated mechanical properties, most notably Interlaminar Shear Strength (ILSS), compressive strength, and fatigue life [1].

For decades, autoclave processing has been refined to mitigate porosity. This is achieved through vacuum application to remove trapped air and the application of high temperature and pressure. The pressure serves to mechanically compress any remaining trapped air, while also increasing the solubility of gases (air, moisture) in the resin, keeping them in solution until the resin polymerises [2].

However, industrial challenges are emerging:

- *Accelerated Manufacturing:* to increase productivity and reduce costs, accelerated manufacturing approach aim to shorten cure cycles. Faster temperature ramps can, however, lead to a rapid viscosity decrease and can also trigger premature gelation, thereby reducing the time available for void removal. In parallel, alternative processes – such as Out-Of-Autoclave (OOA) curing – are also employed to further lower overall manufacturing costs [3]
- *New Material Systems:* advanced material systems are being introduced to meet new performance needs. These include sandwich structures where prepreg composites are assembled with honeycomb cores, or prepregs toughened with thermoplastic nodules. These complex architectures introduce new interfaces and non-uniform flow paths that can trap air, as highlighted by Kermani et al. [4].

These new challenges highlight the primary limitation of existing manufacturing process simulation. Current models are typically macroscopic, treating the composite as a homogenised porous medium and using semi-analytical models to describe bubble evolution. However, these models are simplified models considering bubble as geometry-independent: coalescence and interaction with fibres are not taken into account [5].

To address this gap, a Computational Fluid Dynamics (CFD) approach is used, enabling the modelling and the visualisation of complex fluid flows. This paper presents the extension of a custom, multi-physics solver built in OpenFOAM that couples two-phase compressible flow with the complete thermo-chemo-rheological physics of thermoset curing.

The objective of this work is the development of a predictive tool that can simulate the evolution of bubble populations within realistic microstructures using Representative Volume Elements (RVEs) under classical industrial processing conditions. To achieve this, the paper is divided into two main sections. First, the numerical methodology of the developed solver is presented, with emphasis on the governing equations of the physics involved. Second, the solver is applied to a standard autoclave cycle, demonstrating its capability to capture microscale void dynamics and significantly outperform macro-scale models, which cannot resolve these features.

Numerical Methodology

The numerical framework is developed within the open-source software OpenFOAM version 8, based on the Finite Volume Method (FVM). A custom solver has been extended to capture the complex phenomena occurring during the curing process.

Two-Phase Flow Modelling. The fluid mixture composed of resin (liquid) and void (gas) is modelled as a two-phase, compressible flow. The Volume of Fluid (VoF) method is employed to track the evolution of the resin-gas interfaces. This method solves a transport equation for the phase indicator α, defined as the volume fraction of the resin phase in a given cell:

$$\frac{\partial(\alpha)}{\partial t} + \nabla.(\alpha\, \boldsymbol{U}) + \nabla.(\alpha\,(1-\alpha)\,\boldsymbol{U_c}) = 0. \quad (1)$$

Where $\boldsymbol{U}$ is the velocity vector of the fluid mixture, and $\boldsymbol{U_c}$ is the interface compression velocity. $\boldsymbol{U_c}$ is an artificial velocity added numerically to counteract numerical diffusion of the interface and can be expressed as follows:

$$U_c = C_\alpha |U| \frac{\nabla \alpha}{|\nabla \alpha|}. \quad (2)$$

With C_α the compression factor. The phase fraction $\alpha = 1$ represents a cell filled with resin (liquid), $\alpha = 0$ represents a cell filled with gas, and the interface lies in cells where $0 < \alpha < 1$. The properties of the fluid in any cell (e.g., density ρ, viscosity μ) are calculated as a weighted average (mixture law):

$$\rho = \alpha\, \rho_{resin} + (1 - \alpha)\rho_{gas}.$$
$$\mu = \alpha\, \mu_{resin} + (1 - \alpha)\mu_{gas}. \quad (3)$$

The gas phase (ρ_{gas}) is treated as a compressible ideal gas, while the resin phase (ρ_{resin}) is treated as an incompressible fluid. The effective compressibility of the mixture Ψ_m is therefore expressed as:

$$\Psi_m = \frac{\partial \rho}{\partial p} = (1 - \alpha) \frac{\partial \rho_{gas}}{\partial p} = \frac{1-\alpha}{r\, T}. \quad (4)$$

The core innovation of this work consists in the coupling of the VoF solver with the thermo-chemo-rheological evolution of the thermoset resin. This is achieved by solving three additional, coupled transport equations.

Thermo-Chemical Model (Cure Kinetics). The polymerisation of the thermoset epoxy resin is a scalar field, x, representing the degree of cure (where $x = 0$ corresponds to an uncured matrix, while $x = 1$ to a fully cured one). Its evolution is described by Kamal-Sourour kinetic model [6]:

$$\frac{\partial x}{\partial t} = (k_1 + k_2 x^m)(1 - x)^n \text{ with } k_i(T) = A_i \exp\left(-\frac{E_i}{RT}\right), i = 1; 2. \quad (5)$$

Where m and n are the reaction orders, k_1 and k_2 the rate constants A_i is the Arrhenius pre-exponential factor, E_i is the Arrhenius activation energy, R is the ideal gas constant, and T is the local temperature. This equation is solved as a transport equation for the scalar x within the resin phase.

Rheological Model (Viscosity). The viscosity of the thermoset resin, μ_{resin}, depends on both temperature T and degree of cure x. This behaviour is captured using a modified William-Landel-Ferry (WLF) Castro-Macosko model [7, 8]:

$$\mu(T) = \mu_0 \exp\left[-\frac{C_1\,(T - T_{g0}(x))}{C_2 + T - T_{g0}(x)}\right]\left[\frac{x_{gel}}{x_{gel} - x}\right]^{n_{viscosity}}. \quad (6)$$

With μ_0 being the reference viscosity or initial viscosity before the beginning of cross-linking, T_{g0} the glass transition temperature at 0 % polymerisation, C_1, C_2 and $n_{viscosity}$ material-specific empirical constants, and x_{gel} the degree of polymerisation at the gel point.

Energy Transport and Exotherm. The temperature field T is solved using the energy equation, which accounts for conduction, convection, and the heat source from the exothermic polymerisation reaction:

$$\frac{\partial(\rho T)}{\partial t} + \nabla.(\rho\, \boldsymbol{U}\, T) - \nabla.\left(\alpha_{eff}\, \nabla T\right) + \left(\nabla.(|\phi|\, p) + \frac{\partial(\rho\, K)}{\partial t} + \nabla.(\rho\, \boldsymbol{U}\, K)\right)\left(\frac{\alpha}{C_{v\,resin}} + \frac{1-\alpha}{C_{v\,gas}}\right) = S_{exo}. \quad (7)$$

Where α_{eff} is the effective thermal diffusivity, $C_{v\,resin}$ and $C_{v\,gas}$ are the specific heat capacities for the resin phase and the gas phase respectively, ϕ is the volumetric flux, p is the pressure, and K is the kinetic energy. In practice, additional mass- or continuity-related correction terms originating from the pressure equation may also be included to ensure consistency between the pressure–velocity coupling and the energy equation. The source term S_{exo} represents the exothermal heat of reaction and is only active in the resin phase:

$$S_{exo} = \rho\, H_r \frac{dx}{dt}\,. \tag{8}$$

With H_r the total heat of reaction. This term creates a non-linear feedback loop: the cure reaction releases heat, which increases the temperature, which in turn accelerates the cure rate $\left(\frac{dx}{dt}\right)$, releasing even more heat.

Solver Implementation and Coupling. The custom solver is based on the PIMPLE algorithm, which is a combination of Semi-Implicit Methods Pressure-Linked Equations (SIMPLE) and Pressure-Implicit Split-Operator (PISO) algorithms. PIMPLE algorithm is used to solve Navier-Stokes equations. Basically, at each time step, it performs several pressure corrections loops (such as PISO) within external iterations (such as SIMPLE). PIMPLE algorithm advances the solution in time through iterative prediction of the velocity field, solution of the pressure equation, and subsequent velocity correction, ensuring consistent pressure–velocity coupling at each time step [9]. The result is better convergence and greater robustness for transient or weakly compressible flows, without having to reduce the time step excessively. For this extended solver, at each time step, the following sequence is executed:

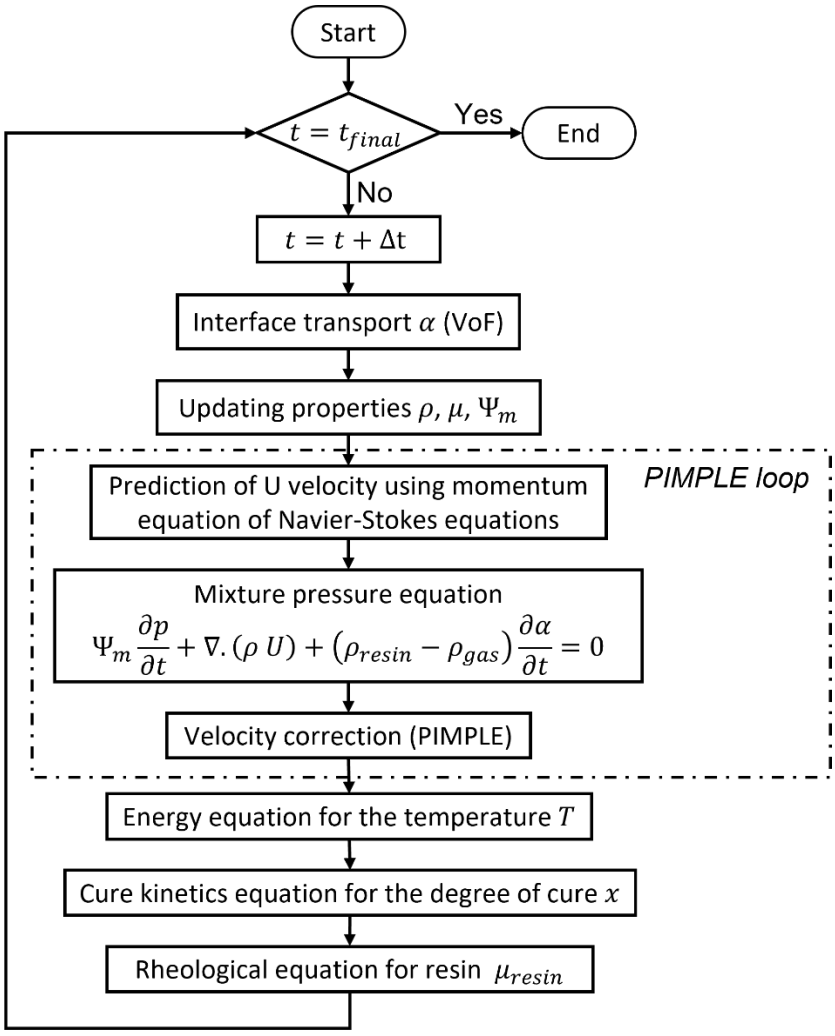

Fig. 1. Algorithm workflow of the extended solver.

Simulation Setup. To represent the composite microstructure, 2D RVEs of a prepreg ply are created using the Digimat® software, which provides a multiscale modeling environment for defining material microstructures. Although the subsequent CFD simulations in OpenFOAM employ a three-dimensional mesh, only a single cell is used through the thickness, effectively reducing the problem to a quasi-2D representation while retaining a 3D framework for solver compatibility. Fibres are modelled as circles (7 μm diameter) with a stochastic distribution, generated to match a specified fibre volume fraction (V_f). In the present case, the RVE has a V_f of 60 %.The fibres are treated as an

absence of mesh with no-slip boundary conditions. No-slip condition and zero pressure gradient are also imposed on the left and right walls, as presented in Fig. 2. This choice represents a first-order approximation that effectively suppresses any motion along the lateral boundaries. Such an assumption remains acceptable in the present configuration, as the flow is essentially quasi-static and no significant pressure-driven filling or strong pressure gradients are involved. The thermal cycle is implemented using a time-dependent Dirichlet boundary condition applied to all boundaries of the RVE. Given the microscopic dimensions of the RVE, the Biot number is significantly low, ensuring that the thermal diffusion time is negligible compared to the process duration. Consequently, the internal temperature field remains effectively uniform, governed by the boundary conditions, while still accounting for the localised exothermic heat source term S_{exo} within the resin phase. The material-specific parameters for the cure kinetics and the rheological model are confidentials and therefore not explicitly reported. However, the framework is designed to be compatible with any standard thermoset system. For reproducibility purposes, representative coefficients for a typical aerospace-grade epoxy resin (such as those for the 8552 or M21 systems available in literature) can be implemented in the simulation case to yield similar qualitative trends in porosity evolution.

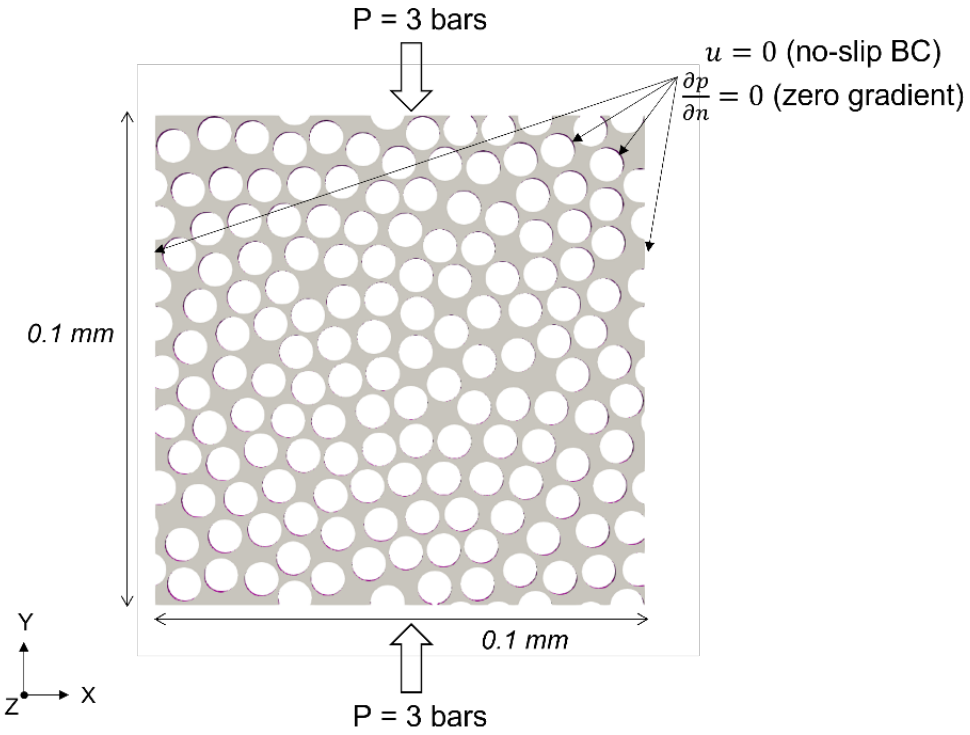

Fig. 2. Example of a RVE of a prepreg ply with the details of the boundary conditions.

An initial population of bubbles (gas phase) is placed in the inter-fibre spaces. To simulate void closure during curing and polymerisation, two types of initial void distribution are implemented, in order to reproduce the initial impregnation on the surface for a prepreg layer, as illustrated in Fig. 3. In the present work, only the band configuration (Fig. 3 (b)) is examined in detail.

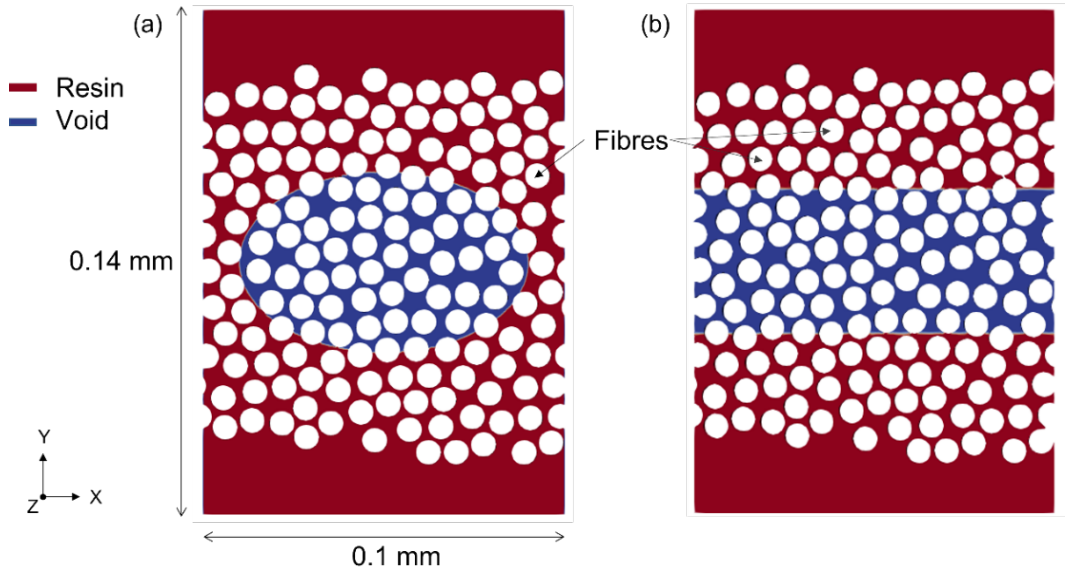

Fig. 3. Two types of initial void distribution reproducing surface impregnation. (a) Oval configuration (not considered in this study), (b) Banded configuration.

Indeed, the fibres at the core are dry before cure and form air evacuation channels, as highlighted by Hu et al. [2]. To simulate an industrial process, time-dependent autoclave cycles are applied. Temperature cycle is applied across the entire domain and a pressure is imposed at the top and bottom of the domain. A typical industrial cure cycle is simulated.

Numerical Verification. A numerical verification was conducted using meshes of up to 140 000 cells per RVE to ensure a high-resolution capture of the fluid interfaces. The study utilised a square cross-section ($0.1\,mm \times 0.1\,mm$) containing approximately 170 fibres to validate the mesh independence. Small timesteps were required to maintain numerical stability and precise resolution of the unsteady-state physics during the 48-hour simulation cycles. The solver, based on the MULES algorithm within OpenFOAM, demonstrated that while parallel efficiency reaches 70-75 % at 16 cores (due to non-scalable portions such as MPI communication and I/O operations), the trends in void compression remain numerically stable across different CPU counts.

Results and Discussion

The developed solver was applied to a RVE with $V_f = 60\,\%$ and an initial void content of $\varepsilon = 20.6\,\%$. The simulations were conducted on a high-performance workstation using 16 cores. A complete process simulation of 15640 seconds requires a computational runtime of approximately 48 hours, representing a manageable cost for high-fidelity micro-scale analysis. Fig. 4 shows a series of snapshots from the simulation, illustrating the dynamic evolution of the void phase (blue) within the resin (red) as it flows around the fibres (white).

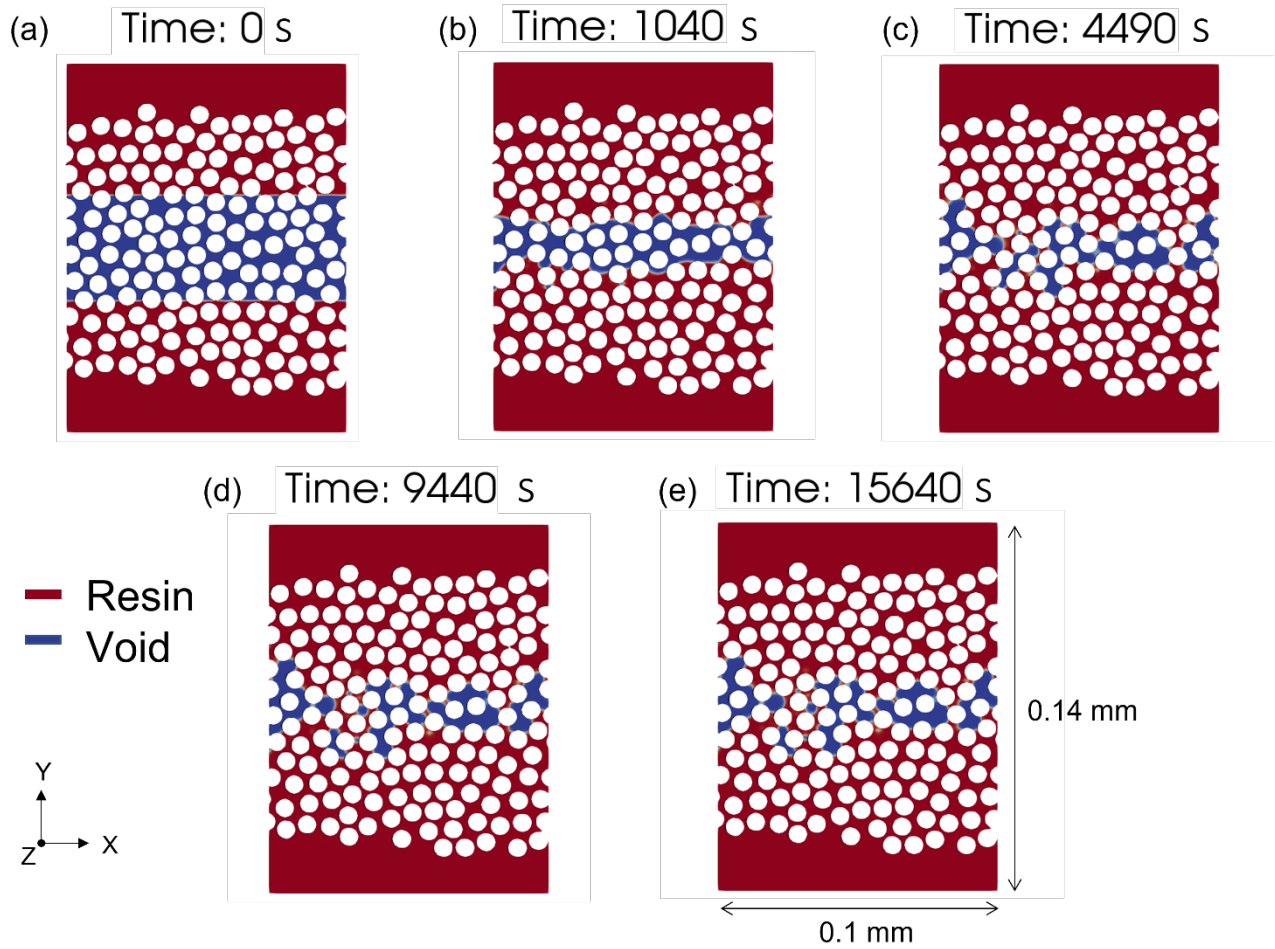

Fig. 4. Time-series of porosity evolution in a 2D RVE ($V_f = 60$ %) during a simulated autoclave cure. (a) Initial state $t_i = 0\ s$, (b) Before viscosity minimum $t = 1040\ s$, (c) Viscosity minimum $t = 4490\ s$, (d) Gelation, $t_{gel} = 9440\ s$, (e) Final cured state, $t_f = 15640\ s$.

- *Initial State* (Fig. 4 (a)): at $t_i = 0$, the void is in its initial configuration, with a banded shape. The resin is at room temperature and has a high viscosity ($\mu = 1.3 \times 10^5\ Pa.s$ for the resin considered here). The autoclave pressure (3 bars) is applied.
- *Heating and Viscosity Minimum* (Fig. 4 (b)): as the temperature ramps up, the resin viscosity decreases, until it reaches its minimum ($\mu = 100\ Pa.s$). The simulation captures the resultant resin flow, which squeezes, deforms, and transports the void. The high external pressure compresses the gas, and the void volume fraction $(1 - \alpha)$ decreases strongly.
- *Curing and Gelation* (Fig. 4 (c)): as the temperature continues to rise, the cure reaction x accelerates. The viscosity begins to rise exponentially as the cross-linking progresses. Once the gelation is reached ($x_{gel} = 0.36$), the pore structure is frozen by the cross-linking of the resin.
- *Final State* (Fig. 4 (d)): once $x \to 1$, the resin becomes a solid and the void does not evolve beyond the gel point. It is frozen in its final, compressed state. The simulation predicts a final porosity $\varepsilon \sim 9$ %.

Fig. 5 plots the key process variables against time.

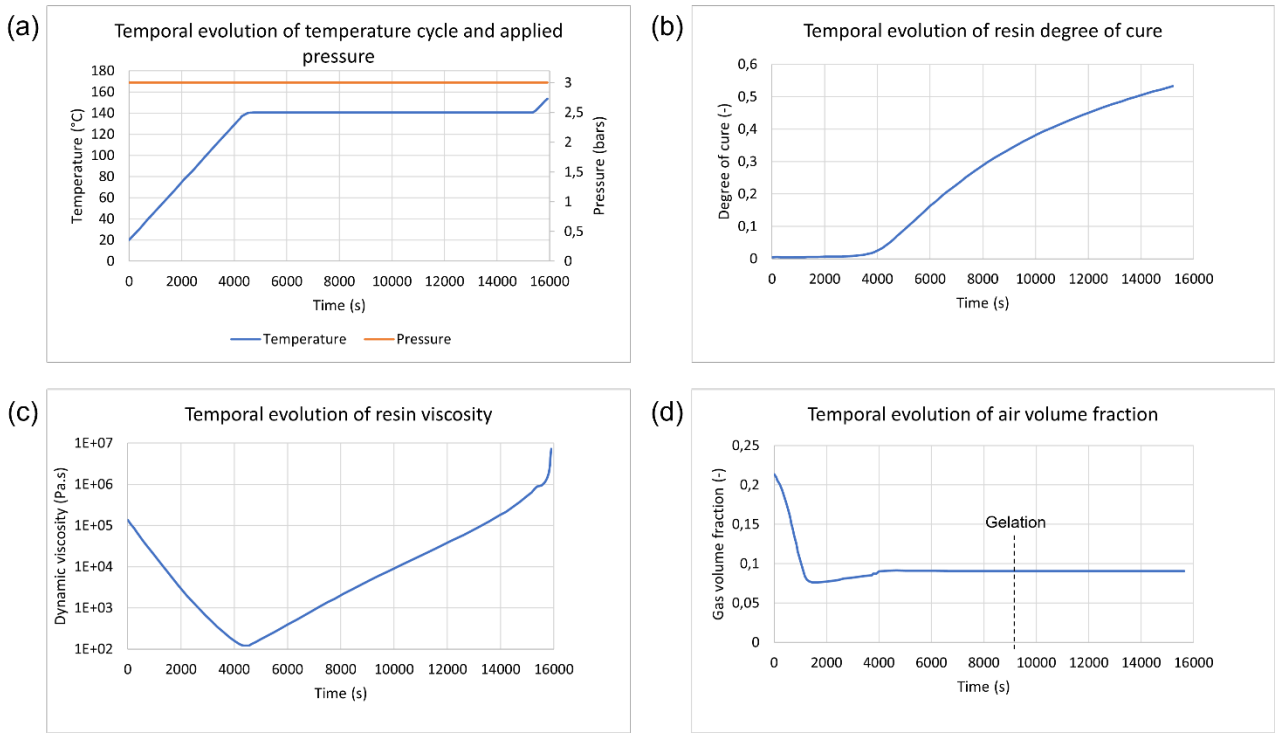

Fig. 5. Process variables versus time. (a) Applied temperature cycle $T_{autoclave}$, (b) Degree of Cure x, (c) Logarithm of the viscosity $log(\mu)$, showing the characteristic V-shaped viscosity profile. (d) Void volume fraction $(1-\alpha)$.

The simulation clearly captures:

1. *The viscosity profile:* The $log(\mu)$ curve shows the characteristic V-shape, dropping due to temperature and then rising sharply due to curing.
2. *Void compression:* The void volume fraction $(1-\alpha)$ drops sharply under autoclave pressure, allowing pressure to be transmitted effectively.

Parametric Study: Effect of Pressure. To demonstrate the model's prediction capability, a higher autoclave pressure is applied. Comparison of the gas volume fraction for 3 bars and 7 bars applied pressure is illustrated in Fig. 6. The informed reader will readily identify that the predicted behaviour is governed by the initial assumption concerning the gas volume fraction; accordingly, the ~4 % residual gas content obtained at 7 bars arises from this modelling choice and must not be interpreted as an inherent upper bound of autoclave consolidation.

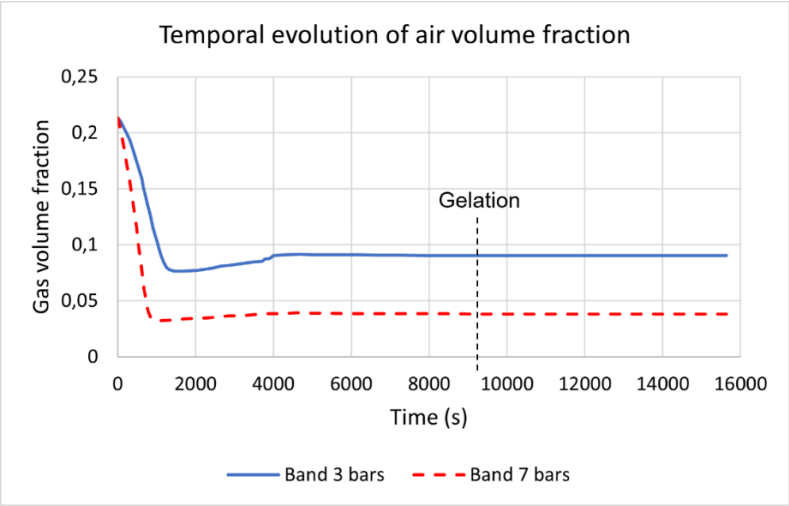

Fig. 6. Comparison of the gas volume fraction for two different values of applied pressure: 3 bars (blue line) and 7 bars (dashed red line).

When a higher pressure is applied, the void phase decreases more significantly, starting from the same initial volume fraction of gas (banded configuration). This shows the importance of autoclave curing: a pressure of 3 bars is typically applied for sandwich panels to prevent crushing the structure, whereas higher pressures of about 7 bars are generally used for laminates.

Conclusions and Future Work

This paper has presented the extension and application of a novel, multi-physics CFD solver framework for modelling porosity evolution at the micro-scale in a thermosetting composite laminate. The key achievements are:

- A custom, biphasic, transient, compressible solver implemented in OpenFOAM by extending an existing solver and enabling full coupling of two-phase flow with cure kinetics, thermo-rheological changes, and the reaction exotherm.
- The simulation of void closure (compression, transport, deformation) within realistic RVEs under industrial autoclave cycles.

However, the model presented in this paper only considers the mechanical compression of pre-existing, trapped air. A major source of porosity, particularly in OOA processing, is the growth of bubbles from dissolved moisture [10]. Therefore, work is underway to incorporate into the solver the phenomenon of moisture diffusion and the physics of mass transport. This involves solving an additional transport equation for the concentration of dissolved moisture in the resin. This additional physics will be introduced coupling the Henry's Law with a Fickian diffusion to model the mass transfer of moisture from the resin into the bubbles. This final feature will allow us to simulate the complete physics of porosity and resin flow in the autoclave-based prepreg manufacturing process at micro-scale.

In order to validate our model, an experimental campaign is planned. This will involve X-ray micro-tomography on semi-cured samples to quantify the 3D void morphology and compare it with simulation predictions. An *in-situ* monitoring of the cure process on a synchrotron beamline is currently under validation. If successful, the latter will provide 4D dataset on bubble evolution that will be used for direct validation of the solver's predictions.

References

[1] M. Mehdikhani, L. Gorbatikh, I. Verpoest, S. V. Lomov, Voids in fiber-reinforced polymer composites: A review on their formation, characteristics, and effects on mechanical performance, J. Compos. Mater. 53 (2018) 1579–1669.

[2] W. Hu, L. Grunenfelder, T. Centea, S. Nutt, In situ monitoring and analysis of void evolution in unidirectional prepreg, J. Compos. Mater. 52 (2018) 1–14.

[3] J.J. Torres, M. Simmons, F. Sket, C. González, An analysis of void formation mechanisms in out-of-autoclave prepregs by means of X-ray computed tomography, Compos. Part A Appl. Sci. Manuf. 117 (2019) 230–242.

[4] N.N. Kermani, P. Simacek, S. G. Advani, Porosity predictions during co-cure of honeycomb core prepreg sandwich structures, Compos. Part A Appl. Sci. Manuf. 132 (2020) 105824.

[5] B. de Parscau du Plessix, S. le Corre, F. Jacquemin, P. Lefebure, V. Sobotka, Improved simplified approach for the prediction of porosity growth during the curing of composite parts, Compos. Part A Appl. Sci. Manuf. 90 (2016) 549–558.

[6] S. Sourour, M. R. Kamal, Differential scanning calorimetry of epoxy cure: isothermal cure kinetics, Thermochim. Acta 14 (1–2) (1976) 41–59.

[7] M.L. Williams, R. F. Landel, J. D. Ferry, The temperature dependence of relaxation mechanisms in amorphous polymers and other glass-forming liquids, J. Am. Chem. Soc. 77 (1955) 3701–3707.

[8] J.M. Castro, C. W. Macosko, Kinetics and rheology of typical polyurethane reaction injection molding systems, Soc. Plast. Eng. Tech. Pap. Annu. Tech. Conf. 38 (1980) 434–438.

[9] C. Greenshields, H. Weller, Notes on Computational Fluid Dynamics: General Principles, CFD Direct Ltd, Reading, UK, 2022.

[10] L.K. Grunenfelder, S. R. Nutt, Void formation in composite prepregs—Effect of dissolved moisture, Compos. Sci. Technol. 70 (16) (2010) 2304–2309.